ACS APPLIED MATERIALS & INTERFACES

Research Article

www.acsami.org

Outstanding H_2 Sensing Performance of Pd Nanoparticle-Decorated ZnO Nanorod Arrays and the Temperature-Dependent Sensing Mechanisms

Chia-Ming Chang,[†] Min-Hsiung Hon,[†,‡] and Ing-Chi Leu[§,*]

[†]Department of Materials Science and Engineering and [‡]Research Center for Energy Technology and Strategy, National Cheng Kung University, 1, Ta-Hsueh Road, Tainan 701, Taiwan, ROC

[§]Department of Materials Science, National University of Tainan, 33, Sec.2, Shu-Lin St., Tainan 700, Taiwan, ROC

Supporting Information

ABSTRACT: The nearly monodispersed Pd nanoparticles with controllable density on ZnO nanorod arrays were prepared by the unique PVP-mediated photochemical deposition (PCD). The changes in morphology and dispersion of Pd on ZnO surface are ascribed to the stabilizing property and self-assembly characteristic of PVP being exploited during PCD. There are three temperature-dependent H_2 sensing mechanisms in those Pd/ZnO NRs, including general oxygen adsorption/desorption mode within 200−300 °C, surface conductivity mode at 60−120 °C and palladium hydride (PdH_x) formation at room temperature, which causes a significant discrepancy in sensitivity variations as a function of Pd density. It is also verified that the electronic sensitization related to the transition of Pd^{2+}/Pd^0 redox couple predominates the promoting mechanism in Pd/ZnO NRs used for sensing H_2 at 200−300 °C. Therefore, the gas sensitivity to 500 ppm H_2 of Pd/ZnO NRs can be significantly improved by around 553-fold (S, R_a/R_g = 1106) at 260 °C through decorating an adequate amount of discrete Pd nanoparticles instead of the Pd clusters, moreover, the corresponding sensitivity at room temperature is 16.9 that is superior to some promising devices reported in the literatures.

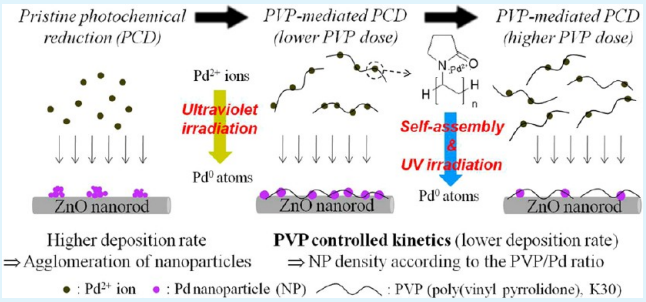

KEYWORDS: *ZnO nanorod arrays, Pd nanoparticle, photochemical deposition, sensing mechanism*

1. INTRODUCTION

The ZnO nanorod/nanowire arrays (NRs/NWs) have been considered as ideal building blocks for high sensitivity gas sensor in virtue of the high surface-to-volume ratio and a readily gas accessible three-dimensional structure. Consequently, ZnO NRs/NWs have been used for sensing various gas analytes, comprising O_2, O_3, H_2, C_2H_5OH, C_3H_6O, CO, NH_3, and so on.[1−7] Among those gases, hydrogen has recently attracted considerable attention as an energy carrier or source for fuel cell. However, there is serious concern about its safe production, storage, and usage because it is explosive when being mixed with air above 4 vol %.[8] Therefore, the effective and accurate detection of hydrogen gas is essential for exploiting it as a renewable energy resource. But the reported sensitivities to H_2 gases in the blank ZnO-based gas sensor are generally not good enough in the literatures[9,10] and the lower sensitivities should be due to the relatively inert surface state for H_2 adsorption on those ZnO nanostructures[11] and the nonpreference to H_2 gases of the ZnO gas sensor by the donating effect.[12] The surface state consisting of surface defects and surface adsorption is highly responsible for gas sensing performance of metal-oxide semiconductor nanostructures[13] and consequently its activity is usually promoted by means of decoration with catalytic noble metals like Pd,[7,14] Pt,[15] Au,[16] Ag,[17] etc. Besides, the palladium not only has a synergistic effect of electronic and chemical sensitization in metal-oxide semiconductor gas sensor,[7,18,19] but also has been commonly used as H_2 sensing material with high sensitivity and selectivity because of its high hydrogen solubility at room temperature.[20,21] Hence, decorating ZnO NRs with Pd nanoparticles is expected to harvest a high-performance H_2 gas sensor.

It is noticeable that the sensing properties of this kind of composite structures are manifestly influenced by the dispersion, size distribution and density of metal nanoparticles on oxide surface.[15,17,22] Yet it is difficult to regulate the size of metal nanoparticles and their distribution on the supporting structures through facile solution-based procedures[23,24] as well as the photochemical deposition (PCD) proposed in our earlier study.[7] Though the gas-phase approaches may give effective ways to tune those features,[17,18] they are stuck with some inevitable drawbacks, such as high processing cost, low yield, and complex adjustment course. Thus it is necessary to exploit

Received: October 11, 2012
Accepted: December 11, 2012
Published: December 11, 2012

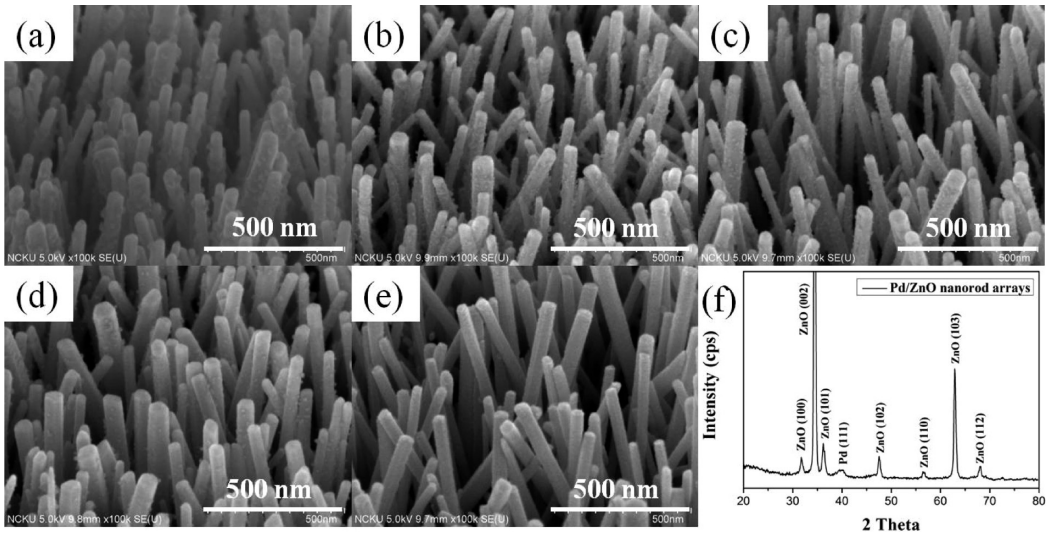

Figure 1. SEM images of Pd/ZnO NRs produced by photochemical deposition (PCD) with (a) 0, (b) 4, (c) 16, (d) 30, and (e) 60 mg of PVP (K30) in 0.25 mM $PdCl_2$-methanol solution. (molar ratio of Pd:PVP = 37−2.5). (f) XRD spectrum of Pd/ZnO NRs fabricated through pristine PCD course.

a facile and reliable strategy for anchoring discrete and uniform Pd nanoparticles on ZnO surface and manipulating the nanoparticle density with ease. Zhang et al.[14,15] have proposed a chemically driven self-assembly method through PVP (polyvinylpyrrolidone) to synthesize noble metal nanoparticles-functionalized ZnO nanowires with uniform particle dispersion, narrow particle size distribution and tunable particle density. And the sensing response to 10 ppm H_2S gas is significantly 34-fold enhanced by decorating adequate amount of Pd nanoparticles on ZnO nanowires.[14] However, this synthetic course[14,15,22] is complex and inconvenient because of its multiple steps, where the noble metal nanoparticles need to be pre-formed and stabilized by ethylene glycol and PVP through polyol technique and sequentially decorated on the supporting ZnO nanostructures. But these studies inspire us to introduce PVP to the PCD process for resolving the problem of nanoparticle agglomeration by its stabilizing property and further controlling the nanoparticle density through modulating the self-assembly characteristic. Therefore, a novel strategy that introduces PVP molecules into the PCD, named as PVP-mediated PCD is proposed in the present study, which enables us to attach discrete Pd nanoparticles onto ZnO NRs and simultaneously alters the nanoparticle density by the amount of PVP addition. The mechanism of morphology and density change of Pd nanoparticles on ZnO surface will also be clarified by the microscopy observations and optical analyses.

The synergistic effect of Pd would promote the sensing properties of ZnO NRs to reducing gas, and the detailed mechanisms are described in an earlier study.[7] The concept related to dual sensitization is extensively reported in the literatures,[18,19,25] but which one dominates the promoting mechanism has not been discussed yet even though it should be better elucidated for further enhancing the sensor performance. Hence, the study on this topic would give a significant impact on the sensor devices involving with this kind of sensitization. Besides, the type of species and quantities of oxygen adsorption are undoubtedly the key factors in the chemical and electronic sensitization, and their variations have been reported to highly depend on the operation temperature.[26] Consequently, the variation in gas sensitivities to H_2 of the Pd/ZnO NRs will be thoroughly discussed in terms of the variation of Pd nanoparticle density and the operating temperature. In the present study, the gas sensitivity to H_2 of Pd/ZnO NRs can be substantially improved at 260 °C through decorating discrete Pd nanoparticles instead of the Pd clusters on the ZnO NRs, in which the effect of transition in Pd^{2+}/Pd^0 redox couple is significantly magnified. In addition, the H_2 sensitivities of the specific Pd/ZnO NRs are remarkably higher than those for other H_2 sensors decorated with metal nanoaprticles[8,19,21,27,28] as a result of the particular Pd nanoparticles that are discretely attached on the functional ZnO NRs with high surface-to-volume ratio.

2. EXPERIMENTAL SECTION

Prior to growth of Pd/ZnO NRs, the pristine ZnO nanorod arrays were grown on the sol-gel derived seed layer through an aqueous chemical growth (ACG) as our previous study.[7] The sol-gel solution was prepared by dissolving and stirring the 2.0 M Zn-$(CH_3COO)_2{\cdot}H_2O$ in the ethanolamine and 2-methoxyethanol solutions at 60 °C for 2 h to yield a homogeneous solution and the molar ratio of ethanolamine to zinc acetate was kept at 1. The sol-gel solution was spun onto the interdigital electrode (Au/Cr around 50/10 nm thickness) with 50 μm gap, and then heated at 300 °C for several minutes for completing the solvent evaporation to form a seed layer. The ZnO nanorod arrays were grown by suspending the seed-coated substrates into the aqueous chemical solution consisting of 0.025 M $Zn(NO_3)_2{\cdot}6H_2O$ and $C_6H_{12}N_4$ at 95 °C for 3 h. The ZnO NRs were washed with distilled water several times and dried at 60 °C in the oven for subsequent noble metal decoration. The decoration of Pd nanoparticles was performed via immersion of the ZnO NRs into the palladium chloride-methanol solution at room temperature and then treated by ultraviolet lamp (365 nm, around 5.3 mW/cm^2) irradiation for 30 min. The palladium precursor solution was obtained by dissolving 0.25 mM $PdCl_2$ and a given PVP (polyvinylpyrrolidone, K30, MW ≈ 40 000) dose in methanol with vigorous stirring for 30 min. In the present study, the mole ratio of Pd to PVP was varied from 37 to 2.5 according to the variation of PVP addition from 4 to 60 mg in the precursor solution. Afterward the Pd/ZnO NRs were acquired through well washing with distilled water and absolute ethanol, blowing with N_2 gas and drying. Finally, the related characterization and measurements of those samples were performed by numbers of apparatuses, including SEM, XRD, TEM, UV−visible, FTIR and gas

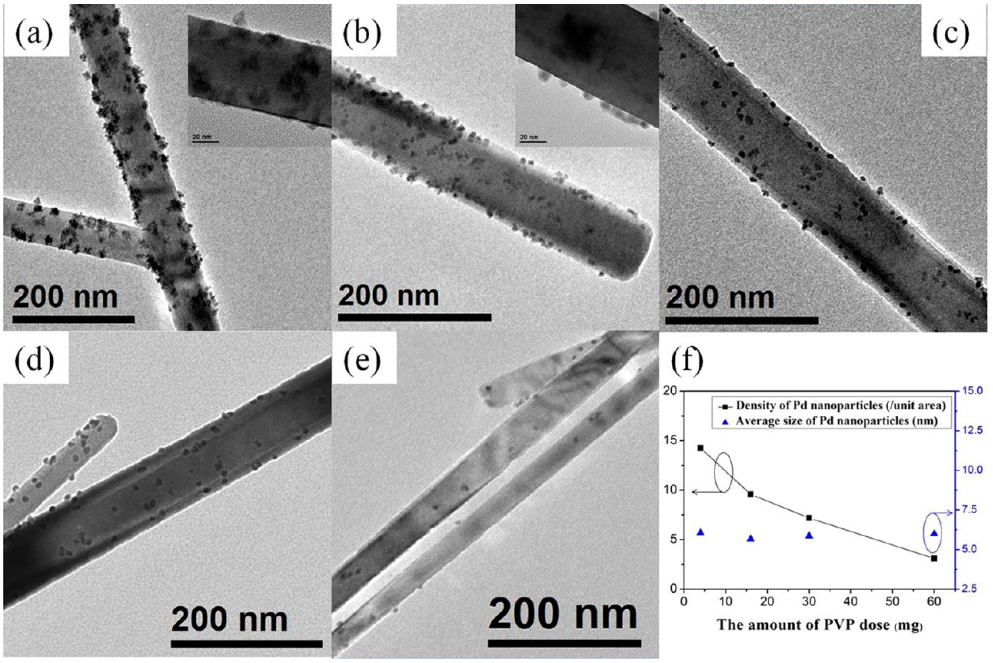

Figure 2. TEM images of Pd/ZnO nanorods produced by photochemical deposition (PCD) with (a) 0, (b) 4, (c) 16, (d) 30, and (e) 60 mg of PVP (K30) in 0.25 mM $PdCl_2$-methanol solution. (f) The variation in density and average size of Pd nanoparticles attached on ZnO nanorods with different dose of PVP addition. (The density is defined as the number of Pd nanoparticles attached onto the surface of cylindrical ZnO nanorod with 50 nm diameter and 100 nm length.)

sensing system, which have been described in detail in the Supporting Information.

3. RESULTS AND DISCUSSION

Fabrication of Pd/ZnO NRs by PVP-Mediated PCD. According to Figure 1, it is exhibited that the palladium nanoparticles are deposited on the ZnO nanorod arrays (NRs) through photochemical deposition (PCD) whether with the addition of PVP or not. And the diameters of ZnO nanorods are nearly unchanged under the growth conditions used in this study. However, the particle sizes of Pd nanoparticles decorated on ZnO NRs by PVP-mediated PCD seem smaller than that produced without PVP addition by comparing their morphologies. This is because the PVP effectively prevents the Pd nanoparticles from agglomerating on the ZnO nanorods' surface. That is a result of the stabilizing (or chelating) characteristic of PVP acting on alleviation of the diffusion rate of Pd(II) ions during Pd NPs deposition. In addition, the amount of Pd nanoparticles (fluffy deposits) on ZnO NRs decreases with the increasing PVP dose in the PVP-mediated PCD processes. The detail mechanism will be described and clarified in the following context. The Figure 1f shows a representative GA-XRD spectrum of Pd/ZnO NRs fabricated by the pristine PCD (without PVP addition), where a diffraction peak at 39.4° is referred to the Pd (111) crystal plane (JCPDS 87-0641) and the other peaks can be well-indexed to the standard pattern of ZnO with wurtzite (hexagonal) structure (JCPDS 36-1451). However, the spectra of Pd/ZnO NRs produced with PVP-mediated course are not shown here because the signals of Pd are indiscernible that could result from the lower density or tiny size of Pd nanoparticles.

For the sake of observing the dispersion of Pd nanoparticles on ZnO nanorod, the TEM images of Pd/ZnO nanorods are taken and shown in Figure 2. It is clearly seen that the morphology of Pd coated ZnO nanorod in Figure 2a differs from the rest of Figure 2, where the nanoparticles are aggregated as small clusters on the ZnO nanorod. As compared with our previous work,[7] the extent of Pd aggregation is obviously alleviated through lowering the concentration of precursor. However, this agglomeration phenomenon cannot be completely ruled out, as shown in the inset of Figure 2a. Accordingly, the multi-functional PVP was introduced into the PCD process for solving this problem via coordination between PVP and palladium ions and the consequent steric effect during the self-assembly course. A significant influence is observed by comparing the insets of a and b in Figure 2, the products come from both the PCD without and with PVP mediator. Besides, there is a replacement of solvent from ethanol to methanol in comparison with earlier study, which is performed to improve the reproducibility and reliability of PVP-mediated PCD process. The related discussion is described in the Supporting Information. In the Figure 2b–e, it clearly shows that the discrete Pd nanoparticles are uniformly distributed on the ZnO surface, and the density of Pd nanoparticles is decreased with the increasing amount of PVP, as shown in Figure 2f. The density is estimated by counting the number of Pd nanoparticles on the ZnO nanorod per unit area. As the graph shows, the density of Pd nanoparticles on ZnO nanorods can be readily controlled from 14.3 to 3.1 according to PVP addition from 4 to 60 mg in this PCD course, respectively. Besides, the average size of Pd nanoparticles in those Pd/ZnO nanorods is nearly 6 nm, which is statistically calculated under a comparable estimated area ($\sim 1 \times 10^5\ \pi\ nm^2$) in each condition. Furthermore, the size distributions of Pd nanoparticles are largely in the range of 3.75–8.75 nm, and the histograms are exhibited in Figure S2a–S2d in the Supporting Information. It indicates that the density-controllable Pd nanoparticle with uniform size could be decorated on ZnO

dx.doi.org/10.1021/am302294v | ACS Appl. Mater. Interfaces 2013, 5, 135–143

NRs by modulating the ratio of $PdCl_2$ to PVP in PVP-mediated PCD.

Figure 3 shows the high-resolution TEM images of Pd nanoparticles on ZnO nanorod, where the particle sizes are at

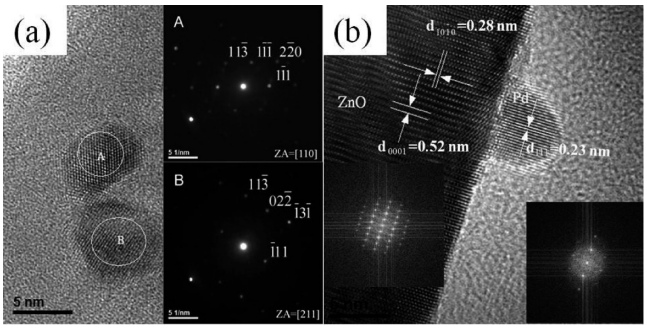

Figure 3. (a) High-magnification and (b) high-resolution TEM images of Pd nanoparticles decorated on ZnO nanorod by PVP-mediated PCD with 16 mg PVP (K30) in 0.25 mM $PdCl_2$-methanol solution. The insets in a and b are the corresponding NBEDs (nanobeam electron diffraction) and FFTs (fast Fourier transform).

around 5 nm. The insets of Figure 3a are the associated NBED (Nanobeam Electron Diffraction) with well-defined diffraction spots, which clearly represent the {111}, {220} and {113} lattice plane of cubic Pd and consequently the single-crystal nature of Pd is confirmed further. The Figure 3b exhibits three definite lattice fringes of 0.28, 0.52, and 0.23 nm spacing, which correspond to the $d_{(10\text{-}10)}$, $d_{(0001)}$ of ZnO, and $d_{(111)}$ of Pd, respectively. It is demonstrated that the Pd nanoparticles are firmly attached on the ZnO nanorod via the PVP-mediated PCD, even the signals of palladium are inadequate to be detected by GA-XRD analysis. That is, the function of PVP addition in the PCD process not only can modulate the density of Pd nanoparticles on ZnO NRs but also can preserve the original crystalline characteristics of Pd/ZnO NRs that produced with regular PCD.

Growth Mechanism of Pd/ZnO NRs through PVP-Mediated PCD. In this section, a plausible mechanism is proposed to account for the influence of PVP on the morphology and dispersion of Pd nanoparticles on the ZnO nanorods, which is based on the relevant discussions with optical analyses in the Supporting information. The density-controllable Pd nanoparticles are decorated on ZnO NRs by PVP-mediated PCD as illustrated in the Scheme 1, and the detailed process is described below. In the pristine precursor solution, the photochemical deposition of Pd nanoparticles on ZnO nanorod is mainly ascribed to the electrostatic attraction and reduction of Pd(II) ions by photo-induced electron carriers.[7] The Pd(II) ions diffuse to the vicinity of the ZnO surface, and adsorb on the ZnO surface through the electrostatic interaction between Pd^{2+} and remaining surface oxygen.[7] And then the Pd(II) ions will be reduced to metallic Pd by the photoelectrons came from the irradiated ZnO nanorod. While adding PVP in the solution, the Pd(II) ions would be coordinated with the unbounded residual N or O atoms of PVP,[15,29−31] forming PVP-Pd^{2+} that is associated with the absorbance peaks in Figure 4a. Thus the viscosity of the precursor solution increases, which causes a decreased diffusion rate of Pd(II) ions (or PVP-Pd^{2+}).[31] This situation will retard the speed of Pd(II) ions anchoring on the ZnO and the subsequent reduction rate. Accordingly, the reduced Pd atoms have a larger probability to grow into the spherical nanoparticles with the thermodynamically favorable critical size for lowering the surface energy. In the Pd/ZnO NRs produced by the pristine PCD, the relatively intensive precipitation of a large amount of Pd nuclei by the reduced Pd atoms comes from the insufficient growth of nanoparticles; as a result, those atoms aggregate as polyhedron shaped particles (or cluster) determined by surface effect.[7] The results of these phenomena are apparently observed in the inset of Figure 2a and 2b. Besides, it is well-known that the PVP have a backbone of polyvinyl as hydrophobic groups and several pendants of pyrrolidone as hydrophilic groups, which separately surround metal particle and interact with water or polar solvent.[30] As the PVP-Pd^{2+} approach to the ZnO by surface charge interaction, the Pd(II) ions coordinated with the pendants of pyrrolidone directly face to the ZnO surface and anchor on it, which causes a spatial repulsion force between adjacent polymer chains due to the hydrophobic property of polyvinyl backbone. This result facilitates the Pd (II) ions to discretely adsorb on the ZnO surface and prevents the reduced Pd atoms from agglomerating. And the PVP-Pd^{2+} could be replenished from bulk solution to ZnO surface after the coordinated Pd(II) ions in PVP have been reduced by photoelectrons and then the unoccupied PVP has detached from ZnO surface by its water-soluble property. This procedure is distinct from the capping of Au or Pt nanoparticles by lysine formed in solution via the reducing agent $NaBH_4$ and simultaneously anchored onto the oxide surface, and consequently has a higher selectivity in metal-oxide support.[16,24] However, the PVP-mediated PCD could sub-

Scheme 1. Schematic Diagrams about the Influence of PVP Addition on the Morphology and Dispersion of Pd Nanoparticles Decorated on ZnO Nanorod via Photochemical Deposition (PCD) Processes

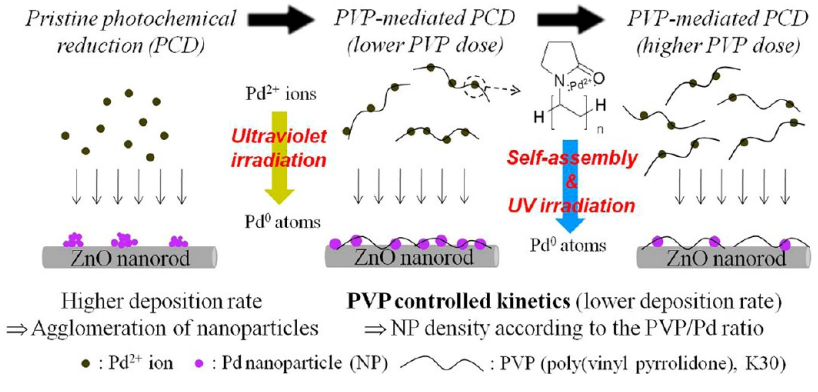

dx.doi.org/10.1021/am302294v | ACS Appl. Mater. Interfaces 2013, 5, 135−143

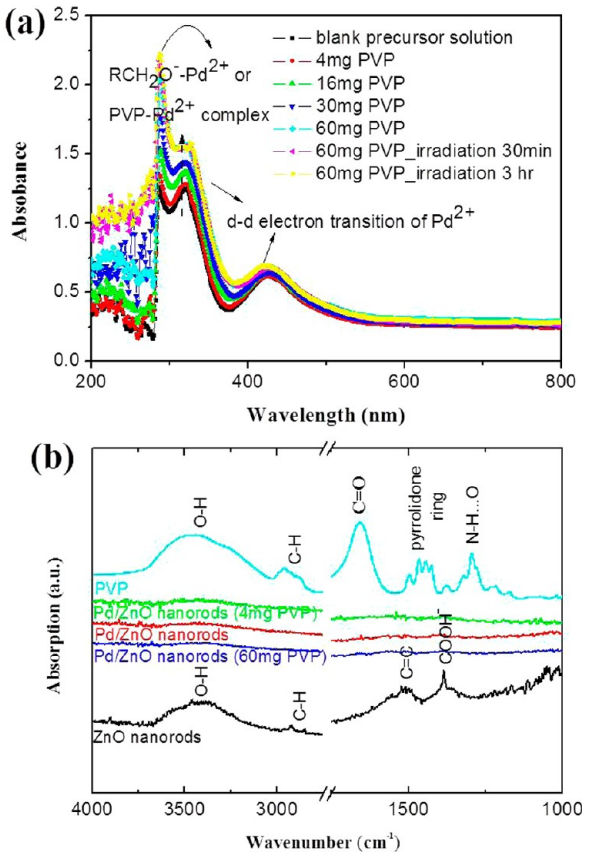

Figure 4. (a) UV−vis absorption spectra of the precursor solution (0.25 mM $PdCl_2$-methanol solution) containing different amount of PVP and that consisting of 60 mg PVP is subsequently irradiated with UV for 30 min and 3 h. (b) FTIR spectra of pure PVP, pristine ZnO nanorods and Pd/ZnO nanorods produced by PCD with different amount (0, 4, and 60 mg) of PVP (K30) in precursor solution.

stantially avoid the unnecessary waste of noble metal salts because the Pd ion are primarily reduced on the ZnO surface by UV derived photoelectrons. The above discussion infers that the PVP could be regarded as a chelating agent (carrier) in this particular process. The role essentially differs from the PVP acting as a linker reagent during decoration of Pt (or Pd) nanoparticles on ZnO nanowires in the literatures,[14,15] where the PVP is radially assembled on the pre-fabricated metal NP and then itself anchors on the ZnO surface. Thus the metal NPs are barely decorated on the surface of ZnO nanowires without PVP linker and the density of NPs is increased with the amount of PVP.[15] These distinct features demonstrate that the functionality of PVP in the present study is different from that in the literatures. Besides, the residual PVP on partial ZnO nanorods can be washed out, which is evidenced by the IR spectra of Pd/ZnO nanorods in Figure 4b. Thus the discrete Pd nanoparticles are decorated on ZnO NRs via this PVP-mediated PCD route and the Pd/ZnO NRs do not need post-annealing before gas sensing analysis. Furthermore, the distribution of Pd nanoparticles on ZnO is found to extremely depend on the amount of dissolved PVP, which is because of the limited solute content that leads to the decreasing numbers of Pd(II) ions coordinated by PVP monomer with the increasing PVP dose. Accordingly, the density of Pd nanoparticles on ZnO is reduced with raising molar ratio of PVP/Pd source. Therefore, a novel strategy is developed to attach density-controllable Pd nanoparticles on ZnO nanostructures surface through one-step solution route at room temperature.

Sensor Performance and Sensing Mechanisms. The variation in gas sensitivity of Pd/ZnO NRs produced with different amounts of PVP at various temperatures is shown in Figure 5 a. The sensitivity is measured during exposure to 15

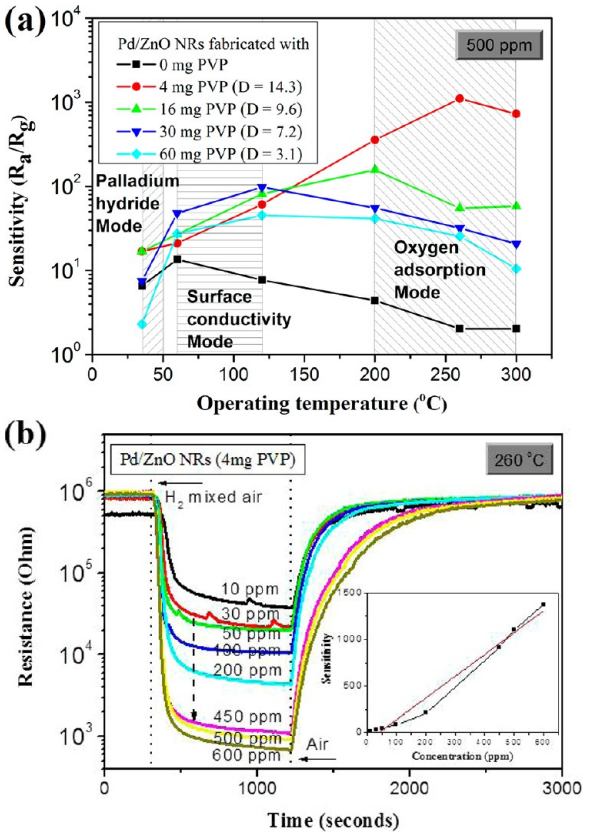

Figure 5. (a) Sensitivity variation of distinct Pd/ZnO NRs used for detecting 500 ppm H_2 mixed air under different temperature. The *D* value in the bracket means the average density (per ZnO nanorod with 50 nm diameter and 100 nm length) of Pd nanoparticles decorated on Pd/ZnO NRs fabricated with different amount (4−60 mg) of PVP. (The sensitivity was measured by exposing to 15 min pulses of specific concentration of H_2 mixed in air as shown in b). (b) Resistance variation of Pd/ZnO NRs fabricated with 4 mg PVP exposed to various concentration (10−600 ppm) of H_2 mixed with air at 260 °C. The inset is the corresponding sensitivity variation versus the concentration of H_2 mixed with air.

min pulses of 500 ppm H_2 mixed in air at respective operating temperatures (as shown in Figure S3a−3e in the Supporting Information), and is defined as the ratio of R_{air} to R_{H2}, where R_{air} and R_{H2} denote the resistances of the Pd/ZnO NRs-based device in air and in the air-hydrogen mixed ambient gas, respectively. Besides, it needs to be reminded that the more PVP addition in Figure 5a represents the less Pd nanoparticles attached on ZnO NRs and the density variation is exhibited in Figure 2f. First of all, the sensitivities of Pd/ZnO NRs increase with the density of discrete Pd nanoparticles at operating temperatures from 200 °C to 300 °C. The sensitivity demonstrating a very high value of 1106 to 500 ppm H_2 of Pd/ZnO NRs (4 mg PVP) is about 43-fold higher than that of Pd/ZnO NRs (60 mg of PVP) at 260 °C. It has been mentioned that there are at least two promoting effects involved in the Pd/ZnO NRs gas sensing operation, that is an

dx.doi.org/10.1021/am302294v | ACS Appl. Mater. Interfaces 2013, 5, 135−143

enlarged amount of oxygen adsorption (O_2 spillover effect) and Pd^{2+}/Pd^0 redox couple transition,[7] and these two effects exhibit a competitive relationship. Using Pd/ZnO NRs for reducing gas sensing, the contribution of O_2 spillover effect (chemical sensitization) and Pd^{2+}/Pd^0 redox couple transition (electronic sensitization) to the improvement in gas sensitivity are highly associated with the amount of adsorbed oxygen and the density of Pd nanoparticles on ZnO surface, respectively. However, the magnitude of activated sites on ZnO surface for oxygen adsorption will be reduced once the number of attached Pd nanoparticles rises, and vice versa. It is reasonable to assume that all of the exposed area of ZnO surface can be the activated sites for oxygen adsorption by the spillover effect of Pd nanoparticles, because the average gap between discrete Pd nanoparticles on ZnO surface in the present study is largely close to the size of spillover zone for oxygen (around 10−100 nm in diameter), as is evaluated for Pd particles on TiO_2 (110) surface using STM[18] (i.e., because the energy band gap and electron affinity for ZnO and TiO_2 are similar). It is commonly reported that both the chemical sensitization and electronic sensitization can be displayed by the presence of Pd NPs. In the present study, we suggest a comparative relationship between these two mechanisms under a Pd NP density-controlled condition, and we can determine the predominant sensitization mechanism through the discussion of the density effect on resistance variation. Based on the above-mentioned results, the electronic sensitization associated with the transition of Pd^{2+}/Pd^0 redox couple predominates the promoting mechanism in the Pd/ZnO NRs used for detecting H_2 in this temperature region. This is because the higher electron donating effect and larger Schottky barrier variation derived from the transition of Pd^{2+}/Pd^0 redox couple than that from the reaction between hydrogen and adsorbed oxygen (O^-) on ZnO surface, as discussed in our previous study.[7] Besides, the O_2 spillover in sensing duration simultaneously compensates the vacant states related to oxygen desorption on ZnO surface, which will discount the influence of adsorbed oxygen quantity (before sensing) on the resistance variation (sensitivity). Thus the chemical sensitization correlated with O_2 and H_2 spillover effect cannot be stood out in the synergistic mechanism at this circumstance. In addition, the sensitivities of Pd/ZnO NRs fabricated by the regular PCD process apparently decrease as shown in Figure 5a, which could possibly result from the aggregation of Pd nanoparticles. The distribution of Pd nanoparticles would severely hinder the oxygen adsorption/desorption over the interfacial Pd crystallite (i.e., those Pd NPs directly contacting the ZnO) and then restraining the influence of Pd^{2+}/Pd^0 redox couple transformation on the Schottky barrier of Pd-ZnO interface. Accordingly, the sensitivities of Pd/ZnO NRs (0 mg of PVP) possessing more Pd clusters are even lower than that of Pd/ZnO NRs (30 and 60 mg of PVP) containing relatively lower densities of discrete Pd nanoparticles. According to the mechanism, there may be Pd/ZnO NRs with optimum Pd nanoparticle density possessing the highest gas sensitivity, and this subject deserves further studies. However, some gas sensitivities to H_2 in the present Pd/ZnO NRs are significantly higher than that of other gas sensors based on noble metal decorated metal-oxide semiconductors. Xiang et al.[27] have reported that the sensitivity to 50 ppm H_2 in Au nanoparticles (0.5 wt %) modified WO_3 nanorods is around 7 at 290 °C; Cho et al[28] have proposed that the response of Pt functionalized SnO_2 hollow hemispheres to 50 ppm H_2 is about 3 at 250 °C. The measured gas sensitivity approaches 45 in the present Pd/ZnO NRs prepared with 4 mg PVP at 260 °C, as shown in Figure 5b. Although the gas-sensor structure and sensing materials are different, the main cause of the discrepancy in sensitivity is believed to result from the synergistic effect of Pd nanoparticles. However, Xing et al.[19] have also fabricated the Pd/ZnO nanoflowers for various reducing gases sensing, and the gas sensitivity to 300 ppm H_2 is only 2.8 at 250 °C. The unexpected lower sensitivity as compared with our results may be due to the larger size distribution and poorer dispersion of Pd nanoparticles, even the Pd nanoparticles are attached on the hierarchical ZnO nanostructure with a high surface area, which would still prohibit the specific electronic sensitization as discussed previously. Therefore, well control of the size and dispersion of noble metal nanoparticles on semiconductor surfaces is extremely important for them to be used for gas sensing. It is manifested by the fact that the H_2 sensitivity can be enhanced more than 550 times at 260 °C by anchoring discrete Pd nanoparticles on ZnO NRs instead of Pd clusters. It also means that the PVP-mediated PCD is indeed a significant and effective methodology for promoting the gas sensing properties in this kind of composites.

In addition, the resistance variations of the Pd/ZnO NRs (4 mg of PVP) used for detecting H_2 gases in the range of 10−600 ppm at 260 °C are shown in Figure 5b, and the corresponding sensitivity increases from 14.2 to 1371 with the raising H_2 concentration, which is plotted in the inset of the figure. As shown in Figure 5b, the resistance of device decreases sharply after introducing H_2 mixed air into the ambience, which is ascribed to the reaction of adsorbed oxygen (O^- or O^{2-}) on Pd/ZnO NRs with the gas analyte and results in the significant reduction of the Schottky barrier height between Pd-ZnO and oxygen depletion layer under ZnO surface. After the resistance approaches to the equilibrium value in the H_2-containing atmosphere, the resistance rises toward the original value as we switched the ambience back to the synthetic air. It can be seen that the equilibrium resistances before sensing reaction have similar values and the variation of response is nearly linear with the H_2 concentration as revealed in the inset, because each sensing cycle is followed by the extraction of remaining gases by pumping and returns to the device's original state. The Pd/ZnO NRs is shown to demonstrate a good reproducibility to H_2 sensing even though it is repeatedly characterized with different concentrations of analyte at a relatively higher temperature (see the Supporting Information, Figure S4). Yang et al.[32] have proposed that the Pd-loaded SnO_2 crystallite fibers exhibit a considerably low detection limit to H_2 gas at 50 ppb, and a sensitivity of 3 can still be obtained to 1000 ppb H_2 at 350 °C. Although the detection limit of Pd/ZnO NRs in this study is merely 10 ppm (sensitivity of 14.2) at 260 °C, the value is far lower than the flammability point of H_2 in air at 4 %.[8] Although limited by our present experimental capability, the real detection limit of Pd/ZnO NRs may be comparable to that in the literatures according to the comparison with sensitivities, and it will be further studied by using more precise apparatus in the near future.

There is a dramatic discrepancy in the Pd density dependence of sensitivity variation in those Pd/ZnO NRs used for sensing H_2 at 60 and 120 °C in Figure 5a. The gas sensitivities of Pd/ZnO NRs initially increase with the PVP dose (decreasing Pd nanoparticles) in the case of PVP-mediated PCD until 30 mg, and then decrease in the Pd/ZnO NRs (60 mg of PVP). It should be due to the different sensing

mechanism predomination or some kinds of phenomena associated with the relatively lower testing temperature. Tsang et al.[33] have reported that the reverse hydrogen spillover processes become an important sensing mechanism at lower temperature (30−200 °C), where the spillover hydrogen species behave like a shallow donor to semiconductor oxide as the direct source of conductivity. This concept has also been reported by a theoretical work, in which the adsorbed hydrogen atoms can act as shallow donor to ZnO directly and furthermore the O−H bonding unit can be regarded as a new type of dopant atom.[34] It sustains the inference that the −OH is the surface site for reversible hydrogen transfer from one location to the other during the H_2 sensing by Pd/SnO_2 in N_2 ambience.[33] Thus the specific H_2 sensing mechanism in the present Pd/ZnO NRs may originate from the modulation in protonic conduction on ZnO surface, which is attributed to the creation/destruction of surface hydroxyl group, and the operating temperature quite coincides with that observed in the literature for the greatest effect of H_2 reverse spillover of 100−200°C.[33] It indicates that the importance of the exposed area of ZnO to resistance variation (sensitivity) in this temperature region is significantly enhanced. Therefore, the gas sensitivities of Pd/ZnO NRs are enhanced with the increasing PVP dose until 30 mg as a result of the larger exposed area of ZnO accompanied by the decreasing Pd nanoparticle density on it. In the meanwhile, the electronic or chemical sensitization related to the O_2 dissociation, adsorption or spillover no longer rule over the sensing mechanism because the efficiency of O_2 spillover significantly descends under 200 °C,[18] but the H_2 spillover effect governs the surface conductivity. According to the above discussions, the H_2 sensing mechanism of the Pd/ZnO NRs in this temperature region is highly associated with the hydrogen storage characteristic of ZnO nanostrucutres,[35,36] thus it can be deduced that the more hydrogen storage capacity leads to the more resistance variation in the gas sensing reaction. Wan et al.[35] have reported that the hydrogen storage capacity of ZnO nanowires was 0.83 wt % at room temperature under a pressure of 3.03 MPa, which is even higher than that of Pd-decorated CNTs in the recent report.[37] However, Chen et al. have also proposed that an adequate number of Pd nanoparticles is essential to provide the optimum number of reaction sites for hydrogen spillover, and excess Pd nanoparticles have an adverse effect on the hydrogen storage performance.[37] The rule can explain the dependence of Pd nanoparticle density on H_2 sensitivity variation in the present Pd/ZnO NRs, and the optimum condition appears in the Pd/ZnO NRs fabricated with 30 mg PVP. Furthermore, the aggregation of Pd cluster would degrade the catalytic activity toward hydrogen spillover[37] and consequently the gas sensitivities of Pd/ZnO NRs synthesized by regular PCD are lower than the others at 60 and 120 °C as well.

Eventually, the Pd/ZnO NRs also can detect H_2 gases at room temperature (~30 °C, RT) in the present study. The H_2 sensing mechanism in Pd decoration-related gas sensors is generally associated with the dissociation of hydrogen molecules over Pd nanoparticles (as a part of H_2 spillover) and dissolution of atomic hydrogen in the Pd nanoparticles.[8,38] Afterward the Pd is changed to palladium hydride (PdH_x) that possesses a lower work function than pure Pd.[8,38] The reduced work function associated with the PdH_x facilitates the transfer of more carriers from Pd nanoparticles to the support underneath, thus causing a more resistance variation in sensing device. This sensing course partially resembles the electronic sensitization caused by the transition of Pd^{2+}/Pd^0 redox couple. But it is substantially different because the oxygen spillover effect by Pd nanoparticles is a thermally activated event,[18] thus the chemisorbed oxygen is greatly diminished at room temperature. On the other hand, the contribution of H_2 spillover to the surface conductivity as well as gas sensitivity reduces with the temperature from 120 to 60 °C. Therefore, the variation of H_2 sensitivity in these Pd/ZnO NRs totally depends on the amount of Pd nanoparticles (or clusters) at room temperature, and the Pd/ZnO NRs (60 mg of PVP) have the lowest response to 500 ppm H_2. In addition, Tsang et al.[33] have also suggested that the palladium hydride (PdH_x) would decompose at around 50 °C and give out the hydrogen species, thus the effect of PdH_x should accordingly descend from RT to 60 °C. Consequently, the magnitude of sensitivity variation from RT to 60 °C in Pd/ZnO NRs (4 and 16 mg of PVP) is less than that of Pd/ZnO NRs (30 and 60 mg of PVP), which just demonstrates the sensors with different major sensing mechanisms at respective testing temperature. It is noticeable that the Pd density dependence of sensitivity variation is slightly different between RT and 200−300 °C, which also demonstrates the diverse sensing mechanism governing the resistance variation by respective dominant factors at different temperature regions. At room temperature, the variation in Pd work function results from hydrogen dissolution in Pd nanoparticle, and thus the morphology of Pd clusters does not affect the sensing response and the Pd/ZnO NRs (60 mg) obtain the lowest sensitivity to 500 ppm H_2. At 200−300 °C, the work function variation is determined by the oxygen adsorption/desorption over Pd surface, so the agglomeration of nanoparticles severely diminishes the effect of electronic sensitization and the smallest sensitivity to 500 ppm H_2 is found for the Pd/ZnO NRs (0 mg of PVP). However, the change of Pd work function by hydrogen dissolution has not been well explained in the literature, and the mechanism remains to be determined. In general, the optimal operating temperatures for these Pd/ZnO NRs are distinct, those of the Pd/ZnO NRs (4 and 16 mg of PVP) with relatively higher Pd density are in the range 200−300 °C, and those of the Pd/ZnO NRs (30 and 60 mg of PVP) with more exposed area of ZnO are at 120 °C. The reason is the diverse sensing mechanism predomination at different temperature regions. Besides, the sensitivity of Pd/ZnO NRs (0 mg of PVP) decreases with raising temperature because the aggregated Pd nanoparticles tend to form a lager cluster and the catalytic activities for H_2 or O_2 gases descend accordingly.

Johnson et al.[8] have exploited the Pd-functionalized multilayer graphene nanoribbon (Pd-MLGN) network for sensing H_2 in N_2 ambience at low temperature. The sensing response to 2000 ppm H_2 of the Pd-MLGN network was measured at the temperature range of 20−100 °C, and the sensitivity increases from 72 % (R_{H2}/R_{air} = 1.72) at 20 °C to 113 % (R_{H2}/R_{air} = 2.13) at 100 °C. The trend of the increasing sensitivity with operating temperature is consistent with most of our results at temperature from RT to 120 °C; nevertheless, the unique sensing mechanism related to the H_2 spillover governing the surface conductivity at 60 and 120 °C is easily ignored under such a normal trend exhibiting in the case of Pd/ZnO NRs without controllable nanoparticle density. Furthermore, the sensitivities of the present Pd/ZnO NRs are outstandingly higher than that of Pd-MLGN network. As shown in Figure 5a, the sensitivity to 500 ppm H_2 in Pd/ZnO NRs fabricated with 4

mg PVP increases from 16.9 at RT to 60.7 at 120 °C. The superior response to H_2 as compared with that of Pd-MLGN network can be attributed to the 3-D structure of nanorod arrays with a relatively higher surface-to-volume ratio, where the analyte gases can diffuse easily throughout the whole sensing material. The sensing kinetics of the present Pd/ZnO NRs is obviously lower than that of Pd-MLGN network, which could result from the underneath seed layer with poorer conductivity than graphene nanoribbon. Recently, Lim et al.[21] have proposed a flexible H_2 sensing device of Pd nanotube arrays (NTs) constructed by a simultaneous dissolution of ZnO NWs templates. Although the whole sensing materials are nearly metallic Pd element, the sensing kinetics is also inferior to that of Pd-MLGN network,[8] which may be attributed to the remaining ZnO seed layer beneath the Pd NTs too. Even though the seed layer hardly participates in the sensing reaction with ambient gases, it still dominates the carriers (signals) collection speed because it acts as a part of electrodes. Accordingly, the sensing kinetics of the Pd/ZnO NRs are expected to be improved by modulating the configuration of seed layer or doping with group 3A cations to increase its conductivity. Nevertheless, the response time of Pd/ZnO NRs (4 mg of PVP) to 500 ppm H_2 at RT and 120 °C is 184 s and 14 s (experimental results are shown in the supporting information Figure S3f), which is significantly less than that of Pd NTs in the literature (i.e., about 280 and 120 s at 25 and 100 °C, respectively). The gas sensitivities to 500 ppm H_2 of Pd/ZnO NRs (4 mg PVP) at RT and 120 °C (16.9 and 60.7, respectively) are nearly 2 and 3.8-fold higher than that of Pd NTs at 25 and 100 °C, that is about 750% (R_{H2}/R_{air} = 8.5) and 1500% (R_{H2}/R_{air} =16) enhancement, respectively. It is demonstrated that the backbone ZnO nanostructure arrays certainly possess a remarkable functionality in supporting Pd for H_2 gas sensor, regardless of the low operating temperature ranges from RT to 120 °C.

4. CONCLUSIONS

In summary, we propose a novel strategy that can easily modulate the density of Pd nanoparticles on the ZnO NRs at room temperature by one-step solution course, and its mechanism is clearly elucidated. This methodology also can be extensively used to construct other functional composites consisting of noble metal decorated oxide semiconductor NRs/NWs for potential applications, like SERs, optoelectronic device and photocatalysts etc. The Pd density dependence of sensitivity variation in those Pd/ZnO NRs is distinct at different temperature region, which is ascribed to the diverse H_2 sensing mechanism predomination. The sensing mechanisms proposed include the oxygen adsorption/desorption on Pd/ZnO surface by H_2 combustion, variation in surface conductivity via H_2 spillover and formation of palladium hydride (PdH_x) through H_2 dissolution. The outstanding H_2 sensitivity, good detecting limit, reproducible property and acceptable response time, are attributed to the specific Pd/ZnO NRs configuration. Therefore, the present Pd/ZnO NRs have a giant potential and advantage for being applicable to the H_2 gas sensor even at the room temperature.

■ ASSOCIATED CONTENT

Supporting Information

Characterization and measurements details, discussions on the replacement of solvent in PCD procedure and relevant spectroscopic analysis, experimental data of size distribution histograms of Pd nanoparticles, several transients of gas response and sensitivity variation for those Pd/ZnO NRs sensors. This material is available free of charge via the Internet at http://pubs.acs.org.

■ AUTHOR INFORMATION

Corresponding Author

*E-mail: icleu@mail.mse.ncku.edu.tw. Fax: 886-6-2380208.

Notes

The authors declare no competing financial interest.

■ ACKNOWLEDGMENTS

The financial support of this study through contracts no. NSC 100-2221-E-006-123-MY3, and NSC 100-2628-E-024-001-MY2 of the National Science Council, Taiwan ROC is greatly appreciated. Thanks to Ms Hui-Jung Shih at National Science Council Instrument Center in NCKU for assistance with FESEM analysis

■ REFERENCES

(1) Wang, J. X.; Sun, X. W.; Yang, Y.; Huang, H.; Lee, Y. C.; Tan, O. K.; Vayssieres, L. *Nanotechnology* **2006**, *17*, 4995−4998.
(2) Liao, L.; Lu, H. B.; Li, J. C.; He, H.; Wang, D. F.; Fu, D. J.; Liu, C.; Zhang, W. F. *J. Phys. Chem. C* **2007**, *117*, 1900−1903.
(3) Park, J. Y.; Song, D. E.; Kim, S. S. *Nanotechnology* **2008**, *19*, 105503.
(4) Zeng, Y.; Zhang, T.; Yuan, M. X.; Kang, M. H.; Lu, G. Y.; Wang, R.; Fan, H. T.; He, Y.; Yang, H. B. *Sens. Actuators, B* **2009**, *143*, 93−98.
(5) Barreca, D.; Bekermann, D.; Comini, E.; Devi, A.; Fischer, R. A.; Gasparotto, A.; Maccato, C.; Sada, C.; Sberveglieri, G.; Tondellod, E. *CrystEngComm* **2010**, *12*, 3419−3421.
(6) Yi, J.; Lee, J. M.; Park, W. I. *Sens. Actuators, B* **2011**, *155*, 264−269.
(7) Chang, C. M.; Hon, M. H.; Leu, I. C. *RSC Adv.* **2012**, *2*, 2469−2475.
(8) Johnson, J. L.; Behnam, A.; Pearton, S. J.; Ural, A. *Adv. Mater.* **2010**, *22*, 4877−4880.
(9) Huh, J. H.; Park, J. H.; Kim, G. T.; Park, J. Y. *Nanotechnology* **2011**, *22*, 085502.
(10) Khan, R.; Ra, H. W.; Kim, J.T.; Jang, W. S.; Sharma, D.; Im, Y.H. *Sens. Actuators, B* **2010**, *150*, 389−393.
(11) An, W.; Wu, X. J.; Zeng, X. C. *J. Phys. Chem. C* **2008**, *112*, 5747−5755.
(12) Zhang, Y.; Xu, J. Q.; Xiang, Q.; Li, H.; Pan, Q. Y.; Xu, P. C. *J. Phys. Chem. C* **2009**, *113*, 3430−3435.
(13) Xue, X.Y.; Chen, Z. H.; Xing, L. L.; Ma, C. H.; Chen, Y. J.; Wang, T. H. *J. Phys. Chem. C* **2010**, *114*, 18607−18611.
(14) Zhang, Y.; Xiang, Q.; Xu, J. Q.; Xu, P. C.; Pan, Q. G.; Li, F. *J. Mater. Chem.* **2009**, *19*, 4701−4706.
(15) Zhang, Y.; Xu, J. Q.; Xu, P. C.; Zhu, Y. H.; Chen, X. D.; Yu, W. J. *Nanotechnology* **2010**, *21*, 285501.
(16) Liu, X. H.; Zhang, J.; Guo, X. Z.; Wu, S. H.; Wang, S. R. *Nanoscale* **2010**, *2*, 1178−1184.
(17) Hwang, I. S.; Choi, J. K.; Woo, H. S.; Kim, S. J.; Jung, S. Y.; Seong, T. Y.; Kim, I. D.; Lee, J. H. *ACS Appl. Mater. Interfaces* **2011**, *3*, 3140−3145.
(18) Kolmakov, A.; Klenov, D. O.; Lilach, Y.; Stemmer, S.; Moskovits, M. *Nano Lett.* **2005**, *5*, 667−673.
(19) Xing, L. L.; Ma, C. H.; Chen, Z. H.; Chen, Y. J.; Xue, X. Y. *Nanotechnology* **2011**, *22*, 215501.
(20) Walter, E. C.; Favier, F.; Penner, R. M. *Anal. Chem.* **2002**, *74*, 1546−1553.
(21) Lim, M. A.; Kim, D. H.; Park, C. O.; Lee, Y. W.; Han, S. W.; Li, Z. Y.; Williams, R. S.; Park, I. *ACS Nano* **2012**, *6*, 598−608.
(22) Xiao, Y. H.; Lu, L. Z.; Zhang, A. Q.; Zhang, Y. H.; Sun, Li.; Huo, L.; Li, F. *ACS Appl. Mater. Interfaces* **2012**, *4*, 3797−3804.

(23) Gou, X. L.; Wang, G. X.; Yang, J.; Park, J. S.; Wexler, D. *J. Mater. Chem.* **2008**, *18*, 965−969.
(24) Liu, X. H.; Zhang, J.; Yang, T. L.; Guo, X. Z.; Wu, S. H.; Wang, S. R. *Sens. Actuators, B* **2011**, *156*, 918−923.
(25) Kumar, M. K.; Tan, L. K.; Gosvami, N. N.; Gao, H. *J. Phys. Chem. C* **2009**, *113*, 6381−6389.
(26) Barsan, N.; Weimar, U. *J. Electroceram.* **2001**, *7*, 143−167.
(27) Xiang, Q.; Meng, G. F.; Zhao, H. B.; Zhang, Y.; Li, H.; Ma, W. J.; Xu, J. Q. *J. Phys. Chem. C* **2010**, *14*, 2049−2055.
(28) Cho, N. G.; Whitfield, G. C.; Yang, D. J.; Kim, H. G.; Tuller, H. L.; Kim, I. D. *J. Electrochem. Soc.* **2010**, *157*, J435−J439.
(29) Shen, Q. M.; Min, Q. H.; Shi, J. J.; Jiang, L. P.; Zhang, J. R.; Hou, W. H.; Zhu, J. J. *J. Phys. Chem. C* **2009**, *113*, 1267−1273.
(30) Zhang, Z. T.; Zhao, B.; Hu, L. M. *J. Solid State Chem.* **1996**, *121*, 105−110.
(31) Zhang, J. H.; Liu, H. Y.; Wang, Z. L.; Ming, N. B.; Li, Z. R.; Biris, A. S. *Adv. Funct. Mater.* **2007**, *17*, 3897−3905.
(32) Yang, D. J.; Kamienchick, I.; Youn, D. Y.; Rothschild, A.; Kim, I. D. *Adv. Funct. Mater.* **2010**, *20*, 4258−4264.
(33) Tsang, S. C.; Bulpitt, C. D. A.; Mitchell, P. C. H.; Ramirez-Cuesta, A. J. *J. Phys. Chem. B* **2001**, *105*, 5737−5742.
(34) Van de Walle, C. G. *Phys. Rev. Lett.* **2000**, *5*, 1012−1015.
(35) Wan, Q.; Lin, C. L.; Yu, X. B.; Wang, T. H. *Appl. Phys. Lett.* **2004**, *84*, 124−126.
(36) Pan, H.; Luo, J. Z.; Sun, H.; Feng, Y. P.; Poh, C.; Lin, J. Y. *Nanotechnology* **2006**, *17*, 2963−2967.
(37) Chen, C. Y.; Chang, J. K.; Tsai, W. T.; Hung, C. H. *J. Mater. Chem.* **2011**, *21*, 19063−19068.
(38) Sun, Y.; Wang, H. H. *Adv. Mater.* **2007**, *19*, 2818−2823.